Successive mechanism of double-proton transfer in formic acid dimer: A classical study

ARTICLE *in* THE JOURNAL OF CHEMICAL PHYSICS · SEPTEMBER 2001

Impact Factor: 2.95 · DOI: 10.1063/1.1398090

Successive mechanism of double-proton transfer in formic acid dimer: A classical study

Hiroshi Ushiyama and Kazuo Takatsuka

Citation: J. Chem. Phys. **115**, 5903 (2001); doi: 10.1063/1.1398090
View online: http://dx.doi.org/10.1063/1.1398090
View Table of Contents: http://jcp.aip.org/resource/1/JCPSA6/v115/i13
Published by the American Institute of Physics.

Successive mechanism of double-proton transfer in formic acid dimer: A classical study

Hiroshi Ushiyama[a] and Kazuo Takatsuka[b]
Department of Basic Science, Graduate School of Arts and Sciences, The University of Tokyo, Komaba, 153-8902 Tokyo, Japan

(Received 5 March 2001; accepted 10 July 2001)

The dynamics of double-proton transfer reaction in formic acid dimer is investigated by performing *ab initio* molecular dynamics simulations. From the viewpoint of optimized energetics alone, the synchronous (simultaneous) proton transfer is more favorable than the successive one. However, a full-dimensional classical dynamics shows that there is a certain time lag, about 8 fs in average, between two proton transfers. When a proton undergoes the first transfer, it moves from an oxygen with higher electron density to the counterpart having the lower one. The proton thus needs an energy sufficient enough to break the chemical bond, resulting in a clime of a potential barrier. On the other hand, the second proton moves from the lower electron-density oxygen atom to the higher one. Hence, the second proton is shifted predominantly by the thus-formed electronic field. Not only due to the time lag observed but mainly because of the difference in the mechanism of transfer, therefore, the present double-proton transfer is identified as successive. A detailed study on dynamics shows that the vibrational modes of the O–C–O skeletons dominate the second proton transfer. © *2001 American Institute of Physics.* [DOI: 10.1063/1.1398090]

I. INTRODUCTION

Multiple-proton transfer (MPT) in hydrogen-bonded systems is one of the most fundamental processes in chemistry and biology. In particular, it is important in oxidation-reduction reactions in many chemical and biological reactions.[1,2] Tautomeric proton transfer in the hydrogen-bonded base pair of DNA (Ref. 3) and proton relay systems in many enzymes are typical examples in biological systems. In the last few decades, various experimental and theoretical studies on single-proton transfer (SPT) in small systems have been reported and analyzed on the basis of few-dimensional potential surfaces.[4,5] However, for a large system, the so-called cooperative motion of atoms consisting of skeletons makes the situation complicated even in a single-proton transfer system. Furthermore, protons in MPT systems interact not only with skeleton motions but also with other protons. Therefore, the physics behind MPT is quite different from that of SPT and little is known about the dynamical mechanism of the MPT process.

One of the latest issues in the experimental studies is the mechanism of double-proton transfer in an *electronically excited state* of 7-azaindole dimer.[6–9] Yet, it is extremely difficult to perform a theoretical analysis on proton transfer in electronically excited states, since plural competing channels parallel with proton transfer can exist. In fact, virtually no theoretical treatise has been made for dynamics of double-proton transfer (DPT) in an excited state with an exception.[10] However, the reality is that the basic mechanism or the theoretical foundation of double-proton transfer even in a ground state is not yet fully clarified. Therefore, we confine ourselves here to the study of a double-proton transfer in a *ground state* only.

To be more specific, we study the mechanism of the DPT in hydrogen-bonded dimer of formic acid in the ground state as one of the simplest systems of multiple-proton transfer. Our goal is to find solutions to the following questions:

(Q1) Do protons transfer simultaneously or successively?

(Q2) What modes dominate the DPT?

(Q3) Are there cooperative tunneling phenomena?

In doing so, we carry out the so-called *ab initio* chemical dynamics applied to the full-dimensional system. Quantum-mechanical tunneling associated with the present DPT will be reported in the next paper.

Almost all the previous papers studying the DPT in formic acid dimer (FAD)[11–19] concern construction of (reduced) one- or few-dimensional potential surfaces to estimate the energy of the transition state.[11–14] Although different levels of calculation give different barrier heights, the concerted (synchronous) reaction mechanism has been commonly suggested from the viewpoint of energetics alone. Recently, Kohanoff *et al.* have performed an *ab initio* chemical dynamics with fixed O–O bond lengths and investigated the solvent effect on DPT in FAD.[19] They have pointed out that the motion of two protons is not fully synchronized. However, their study is still limited in that the O–O bond lengths, which are likely to dominate the dynamics, were fixed in their scheme. To clarify the reaction mechanism, a full-dimensional dynamical study with no fixed mode is required.

This paper is organized as follows. To see the outline of the present DPT, we first draw two-dimensional potential surfaces in two different extreme cases in Sec. II. Computational details are summarized in Sec. III. The dynamics of the DPT in FAD is presented to answer (Q1) in Sec. IV. We

[a]Electronic mail: ushiyama@mns2.c.u-tokyo.ac.jp
[b]Electronic mail: kaztak@mns2.c.u-tokyo.ac.jp

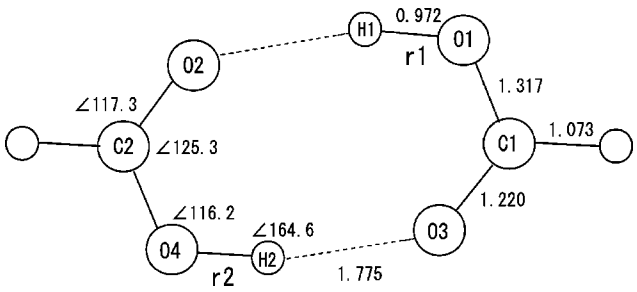

FIG. 1. The optimized geometry of formic acid dimer in units of degree and angstrom.

study the reaction mechanism of DPT in great detail and answer (Q2) in Sec. V. This paper concludes with some remarks in Sec. VI.

II. POTENTIAL SURFACES

We first examine the energetics to see the outline of the DPT in FAD. The optimized structure of FAD which has C_2 symmetry is shown in Fig. 1. Bond distances and bond angles are presented in angstroms and degrees, respectively. The electronical energy has been calculated with use of the restricted Hartree–Fock (RHF) method with the 6-31G basis set in the GAMESS package. The ground-state energy of the optimized structure has been found to be $-10\,268.49$ eV. This energy is about 40 eV higher than that given by the higher level calculations.[14] In what follows, all the energies are to be measured from the thus-obtained global minimum. We have also examined the potential energy surface produced by the MP2 (the second-order Møller–Plesset perturbation theory) level calculation. Although the lowest energy, the saddle-point energy, and so on are quantitatively different from those obtained by means of the Hartree–Fock method, the potential profiles along the so-called minimum energy paths have been found to be qualitatively equivalent to each other. In spite of the fact that the electron correlation is important in this system, we remain at the Hartree–Fock level throughout this paper, since the higher approximations require a huge computational time for chemical dynamics.

We draw two-dimensional potential energy surfaces (PES) to describe the ground-state double-proton transfer reaction as a function of O1–H1 distance ($r1$) and O4–H2 distance ($r2$) in Fig. 2. Two extreme cases are exhibited there. One is the so-called ''adiabatic'' or ''slow-flip'' approximation, and the other is the so-called ''sudden'' or ''frozen bath'' approximation. In the adiabatic approximation, protons are supposed to move much slower than the other particles and the motions of the skeletons adjust adiabatically. On the other hand, the sudden approximation assumes that the protons move so much faster than the other particles that the skeletons are geometrically frozen during the proton transfer.

The PES and its contour plot for the adiabatic approximation is shown in Fig. 2(a). In the case of the adiabatic approximation, the bond lengths of $r1$ and $r2$ range between 0.9 Å and 1.5 Å. For each pair of $r1$ and $r2$, the geometries of the other atoms are optimized. There are two minima on PES in Fig. 2(a) corresponding to the equivalent geometry. The so-called minimum energy path (MEP), which connects the two minima, is also shown as a dashed line. Along the MEP in Fig. 2(a), the concerted motion is more favorable than the stepwise (successive) proton transfer on this PES. The transition-state energy in Fig. 2(a) has been found to be 0.68 eV in the present calculation.

Figure 2(b) shows PES and its contour plot for the sudden approximation. Only $r1$ and $r2$ are varied, with all the other geometries kept frozen. In this case, there are two different kinds of minima on PES and the system is no longer of C_2 symmetry. The potential energy of the lower minimum is, of course, equivalent to the optimized structure in Fig. 2(a). An MEP connecting them is drawn with a dashed curve. The energy of the higher minimum is 1.63 eV, and that near the intermediate region along the reaction coordinate ($r1 \simeq 1.8$ and $r2 \simeq 1.0$) is 1.90 eV. No reaction intermediate having a local minimum is found, though. The energy at the transition state, where $r1=1.8$ and $r2=1.4$, is as high as 2.17 eV, which is 1.49 eV higher than the saddle energy in the adiabatic approximation. Within the sudden approximation, a successive mechanism is more favorable than the concerted mechanism: one of the protons transfers first and then

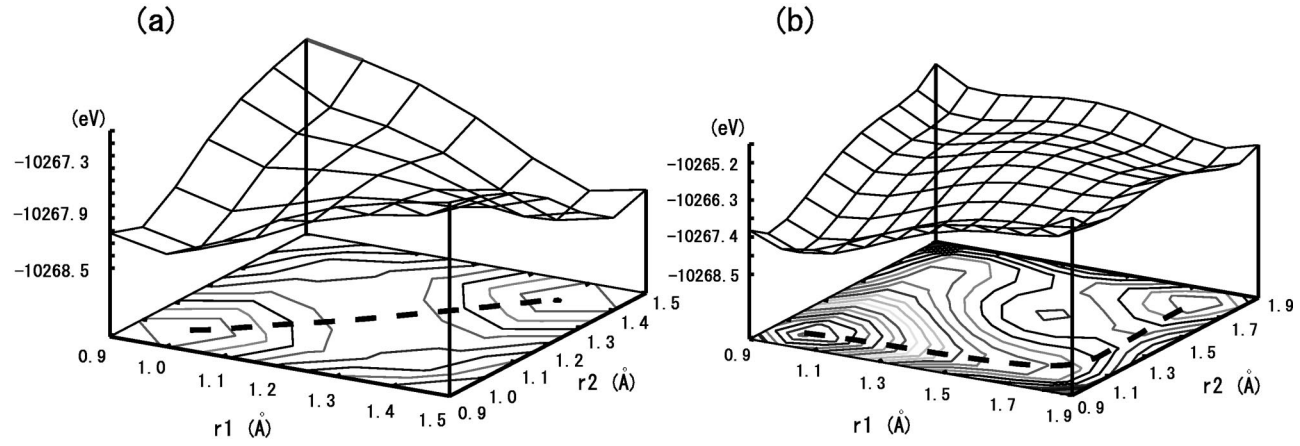

FIG. 2. Two-dimensional potential surfaces in (a) the adiabatic approximation and (b) the sudden approximation.

TABLE I. Energy profiles of the FAD system.

	Energy (eV)	Energy from the bottom (eV)
Optimized energy	−10 268.5	0.00
Saddle-point energy (adiabatic case)	−10 267.8	0.68
Saddle-point energy (sudden case)	−10 266.3	2.17
Zero-point energy	−10 266.5	2.04
Formation energy	0.82	···

the other one moves with some time lag. The energetics data are summarized in Table I.

Upon comparison of Fig. 2(a) with Fig. 2(b), from the viewpoint of energetics alone, it seems that the concerted reaction mechanism is far more favorable than the successive occurrences. It is a usual practice that the reaction path is determined with use of the adiabatic or sudden approximation. However, it is neither expected generally that neither the motion of the light proton is slow enough nor that the motions of the other heavy atoms are frozen during proton transfer. Therefore, the real dynamics of the DPT in FAD should be in between the above two extreme cases. A full-dimensional calculation is thus required to study the real dynamics.

III. COMPUTATIONAL DETAILS

In our *ab initio* chemical dynamics simulation without generating a global PES, all the vibrational freedoms are dealt with on an equal footing with no fixed mode. The potential derivatives have been yielded with the RHF method of the 6-31G basis set in the GAMESS package. The equations of motion were integrated using the so-called locally analytic integrator (LAI) with an integration time step of 0.5 fs.[20] LAI solves ordinary differential equations by recasting them into a set of nonlinear equations and an individual solution is represented in terms of an analytic function of time for an individual short interval, the parameters of which are to be determined in an iterative manner. LAI is an efficient integrator, especially for classical and semiclassical calculations in molecular systems.[20]

We first sampled the position of each atom $\mathbf{R}_{\text{init}}$ randomly around the optimized position of each atom $\mathbf{R}_{\text{opt}}$, keeping $|\mathbf{R}_{\text{init}}-\mathbf{R}_{\text{opt}}|<0.2$ Å. Two hundred initial points were selected as starting positions of trajectories. Each trajectory was integrated with zero initial momenta. After 10 fs of running, we reset both the total translational and angular momenta to zero. The internal momenta are scaled so as to attain the following total energies: $E=0.54,0.81,1.08,\ldots,4.35$ eV. We regard these positions and momenta as initial conditions of trajectories. Each trajectory runs 150 fs, which is long enough to study the DPT reactions.

Since the initial total energy was distributed into all the possible vibrational modes, the system does not undergo an immediate reaction. Frequent proton transfer has not been observed either, even at a high energy. For instance, the ensemble of sampled trajectories having an energy as low as $E=1.90$ eV has only 24 single-proton transfers (SPT) and 5 double proton transfers (DPT), while 144 SPT and 74 DPT occurred in the collection of those trajectories of $E=4.35$ eV.

IV. BASIC TIME SCALES OF THE DOUBLE-PROTON TRANSFER

We first study the basic time scales of the proton transfers, which should be helpful to find an answer to question (Q1). To do so, let us define relative coordinates to specify the position of protons in between the two formic acid molecules such that

$$\eta_1=R_{\text{O2–H1}}\cos(\theta_{\text{O1–O2–H1}})/R_{\text{O2–O1}},$$

$$\eta_2=R_{\text{O4–H2}}\cos(\theta_{\text{O3–O4–H2}})/R_{\text{O4–O3}},$$

where $R_{\text{O2–H1}}$ is, for example a distance between the atoms O2 and H1 in Fig. 1, and $\theta_{\text{O1–O2–H1}}$ is an angle between the lines O2–O1 and O2–H1. $\eta_1>0.5$ and $\eta_2<0.5$ imply that H1 and H2 stay at O1 and O4 sides, respectively. At the optimized structure, η_1 and η_2 are about 0.65 and 0.35, respectively. $\eta=0.5$ is regarded as a threshold value to judge that a proton transfers from one side to the other. When both η_1 and η_2 exceed 0.5 simultaneously, we regard that they undergo transfer in a concerted manner.

A. Time lag between the two proton transfers

Two typical time series are exemplified in Fig. 3, picked from two selected trajectories of an energy 2.99 eV [panel (a)] and 4.35 eV [panel (b)]. We first look at the time dependence of η_1 and η_2 for the low-energy trajectory, Fig. 3(a). In this example, only a single DPT is observed, where η_1 crosses $\eta=0.5$ line at $t=29$ fs indicating the transfer of H1, and at $t=42$ fs the second proton transfer made by H2 follows. The time lag between them is about 13 fs. After this DPT, the dimer dissociates, leaving η_1 and η_2 far from the line of $\eta=0.5$.

Figure 3(a) also exhibits the periods of the vibrational motions of protons. Before crossing the line $\eta_1=0.5$ ($\eta_2=0.5$), η_1 (η_2) oscillates with an period about 17 fs (10 fs), and it turns to 10 fs (17 fs) afterwards. This clearly reflects the change of strength of the bonds.

We next see the behavior of the trajectory of a higher energy [Fig. 3(b)], which shows much more frequent double-proton transfers. An interesting characteristic is noticed in the ordering of shifted protons: The second-transferred proton in a DPT event turns to the first-transferred proton in the next DPT. Thus, the order of the protons undergoing transfer looks like {H1,H2,H2,H1,H1,H2,H2, . . . }. We currently have no idea whether this is a general rule or not. In the example of Fig. 3(b), such DPTs occur four times before being terminated by a single-proton transfer. We notice again that there is certainly a time lag between the first- and the second-proton transfers, whose length is as long as about 8 fs on average.

B. Successive occurrences of proton transfers

The examples of reaction path shown in the last subsection have displayed clear time lags, suggesting a stepwise reaction. To confirm that they are not exceptional, we show in Fig. 4 a frequency histogram at the energy $E=4.35$ eV in

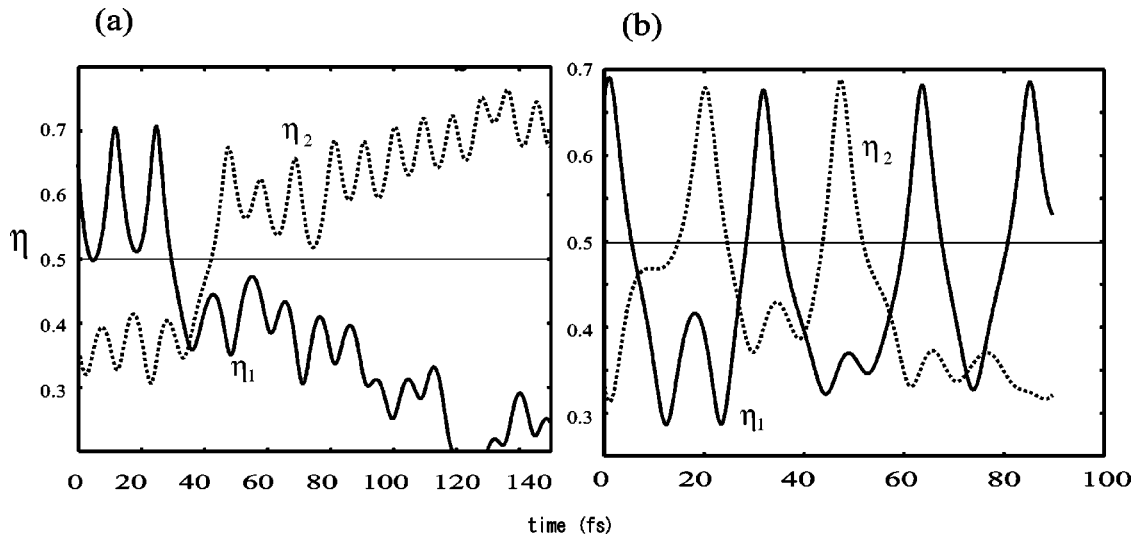

FIG. 3. Examples of selected classical paths: (a) a path with $E=2.99$ eV and (b) a path with $E=4.35$ eV.

which the distribution of position of H2 (η_2) is depicted at a time when H1 happens to be located at $\eta_1=0.5$ on the way of its transfer. This histogram has been made up over the sampled trajectories and the time-series data arising from individual trajectories like Fig. 3. This type of distribution is more or less common to other cases of energy above the threshold. If the two protons move concertedly, the position distribution of the first proton should have a peak at $\eta_2=0.5$. However, it has two peaks located at around 0.38 and 0.62, which are, respectively, close to the values arising from the optimized structure, 0.35 and 0.65. Figure 4 therefore indicates that when H1 is at the critical position $\eta_1=0.5$, the proton transfer due to H2 is already over or it has come back to the original side after recrossing $\eta_2=0.5$. It is true that a minor distribution at $\eta_2=0.5$ is observed. However, this is very exceptional. On the contrary, one can conclude that the majority of the present double-proton transfers has occurred in a successive manner.

C. Energy dependence of the time scales

We next investigate the energy dependence of the relevant time scales. The time lag is well defined as the difference between a time when the first proton crosses the critical region $\eta=0.5$ and that when the second one comes across the critical line. Let us next define an induction time of the successive double transfers by a time taken from the second proton transfer to the first one in the next DPT. That is, the difference between the ''finishing time'' of a second proton transfer and the ''initial time'' of the next double-proton transfer.

To see their energy dependence, we show the induction time (solid line) and the time lag (broken line) as functions of the total energy in Fig. 5. In the present simulation, the number of sampled trajectories is not large enough to have a full convergence in the statistics. Nonetheless, one can deduce a qualitative conclusion from this figure: The total induction time becomes shorter as the energy is raised, while the time lag remains virtually unchanged. This implies that the first proton transfer is accelerated by the energy, but the second one is not. It is therefore suggested that the first proton transfer is promoted by a thermal factor to surmount a barrier, while the second proton transfer should take place under a static circumstance.

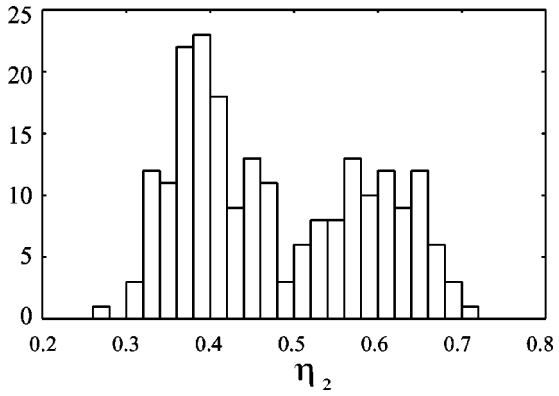

FIG. 4. A frequency histogram of the position distribution of H2 (η_2) at a time when H1 makes a transfer ($\eta_1=0.5$).

V. MECHANISMS OF THE DOUBLE-PROTON TRANSFER

We now explore the mechanism of the present proton transfers to find an answer to question (Q2). In what follows, we investigate the difference between the mechanisms of the first- and second-proton transfers in a single DPT. For the sake of convenience in presentation, we simply refer to the first (secondary) transferring proton as H1 (H2), as assigned in Fig. 1, no matter whether it is actually H1 (H2) or not. (If H2 happens to be the first proton in a DPT, simply rename all the atoms, including the skeleton atoms, according to this convention.) We redefine the relative coordinates of the positions of the protons as before. That is

$$\xi_1=R_{\mathrm{O2-H1}}\cos(\theta_{\mathrm{O1-O2-H1}})/R_{\mathrm{O2-O1}},$$

$$\xi_2=R_{\mathrm{O4-H2}}\cos(\theta_{\mathrm{O3-O4-H2}})/R_{\mathrm{O4-O3}}.$$

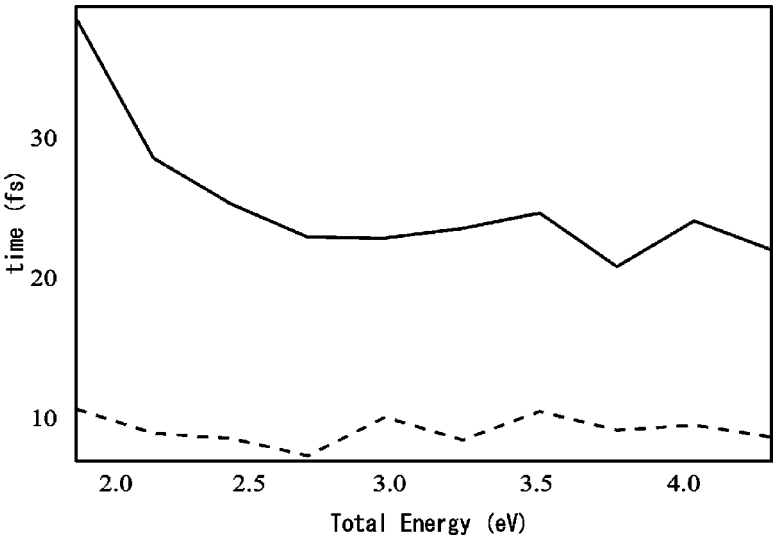

FIG. 5. Energy dependence of the time lag between the first- and second proton transfers and the induction time (see the text).

Note that ξ_1 (ξ_2) is not necessarily the same as η_1 (η_2) in a strict sense.

A. The first proton is pushed thermally

A simple geometrical condition for the first proton transfer to take place is studied in terms of the inner product (the maximum value scaled to unity) between the O1–H1 velocity vector and the O1–O2 position vector. A frequency histogram for the averaged inner product taken at unspecified timings over the sampled trajectories is shown in Fig. 6(a). The values of the inner product are widely spread over the entire possible range, suggesting that these vectors form random angles.

If we make a histogram of the same kind taken only at incidences of $\xi_1=0.5$, quite a different pattern is observed as in Fig. 6(b). A sharply biased distribution at the value unity clearly indicates that the velocity vector of O1–H1 should lie mostly parallel to the direction of O1–O2 for the first proton transfer to be possible. This figure therefore suggests that the first proton transfer is induced thermally against a potential barrier. This aspect will be confirmed below by looking at the change of the potential energy along the reaction coordinate.

B. Potential-energy change during the transfers

Let us explore dynamical factors that primarily dominate the dynamics of double-proton transfer. Figure 7 displays a change of the potential functions along a trajectory that was exemplified in Fig. 3(a). Panel (a) shows $\xi_1(t)$ and $\xi_2(t)$ as a reference to identify the relative positions of protons. At about $t=29$, at which $\xi_1=0.5$, the first proton passes over its critical position, and at $t=42$ the second proton goes beyond its critical position $\xi_2=0.5$. Panel (b) in Fig. 7 exhibits, synchronously with panel (a), the change of the total potential energy V_{total} along this trajectory. It is seen that the trajectory climbs the potential barrier by the time of $\xi_1=0.5$ to accomplish the first proton transfer, while it falls from the top of the potential down to the place of $\xi_2=0.5$ before the second proton transfer. It is about $t=38$ when V_{total} takes the maximum. Thus, this figure strongly suggests a significant difference in the mechanism between the first- and second proton transfers.

We further investigate what happens to the individual protons. To see it, potential fields felt by the first proton, $V_{\text{local}}(\text{H1})$, are calculated with an expression

$$V_{\text{local}}(\text{H1})=\langle\Phi_{\text{elec}}|\sum_{i=1}^{\text{electron}}\frac{-e^2}{r_{\text{H1},i}}|\Phi_{\text{elec}}\rangle+\sum_{A\neq H1}^{\text{nuclei}}\frac{Z_A e^2}{R_{\text{H1},A}}, \quad (1)$$

where Φ_{elec} is an adiabatic electronic wave function at a given nuclear configuration. $r_{\text{H1},i}$ and $R_{\text{H1},A}$ are a distance between the proton H1 and, respectively, an electron i and the other nuclei A with an atomic charge $Z_A e$. The potential applied on the second proton $V_{\text{local}}(\text{H2})$ is given in a similar way. Figure 7(c) shows $V_{\text{local}}(\text{H1})$ and $V_{\text{local}}(\text{H2})$ along the

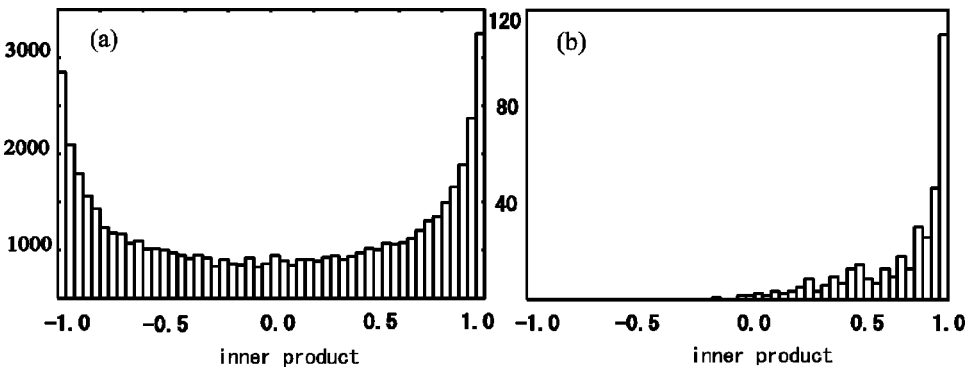

FIG. 6. Distribution of the inner products of the O1–O2 position vector and the O1–H1 velocity vector are displayed; (a) values averaged over unspecified timings; (b) those taken only at incidences of the first proton transfer at $\xi_1=0.5$.

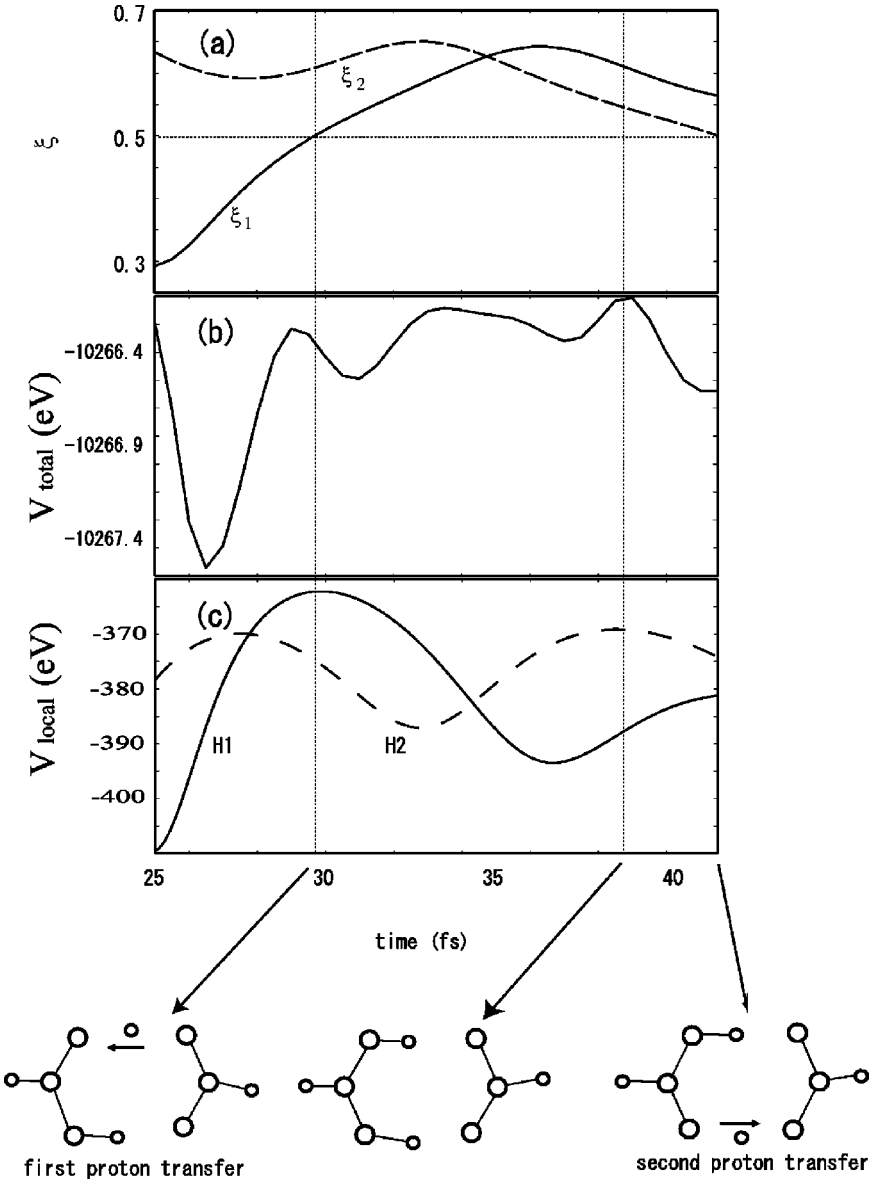

FIG. 7. Change of the potentials along a trajectory. (a) Positions of protons ξ_1 and ξ_2 as a function of time along the classical path shown in Fig. 3(a). (b) Total potential energy V_{total}. (c) Potentials working on H1 and H2.

trajectory. This figure clearly identifies the physical origin of change of the total potential in Fig. 7(b): The first proton transfer occurs by surmounting the potential barrier [curve H1 in Fig. 7(c)]. After a fluctuation, the potential working on the second proton begins to lower at about $t=38$, pushing it down to the critical position $\xi_2=0.5$. Thus, these figures are evidence that the driving forces of the first- and second-proton transfers are different: The first one is characterized as a thermal reaction climbing a potential barrier. On the other hand, the second proton seems to be pulled down from the summit of the potential barrier as though attracted by a potential field. The basic profiles of these types of the potential-energy change are generic and identified in a more or less similar fashion as other trajectories.

C. The second proton is pulled by the electronic charge

To clarify what causes the potential lowering as observed in Figs. 7(b) and 7(c) before the second proton passes through the critical point $\xi_2=0$, we look at the electron density on the skeleton atoms.

First, let us define a difference of the electron densities on the oxygen atoms O4 and O2 that sandwich C2 of formic acid in a left hand side (see Fig. 8). O2 accepts the first proton and O4 is going to donate the second proton. We want to see the change of the electron density after the first proton transfer by tracing $E_{\text{O4}}-E_{\text{O2}}$, where E_{O4} is, for instance, the so-called Mulliken population on the oxygen atom O4; see Fig. 9(a). At the initial structure, the electron density of O2 is lower by 0.1 than that of O4; that is, $E_{\text{O4}}-E_{\text{O2}}=0.1$. This is simply because the hydrogen atom renders its partial electron density to the chemically bonded oxygen atom (O4). Thus, Fig. 9(a) begins with a value similar to such a value for $E_{\text{O4}}-E_{\text{O2}}$ and it remains positive even after the first proton transfer is accomplished. However, at a time $t\sim 38$, when both V_{total} and V_{local}(H2) come to their maximum, $E_{\text{O4}}-E_{\text{O2}}$ turns out to be negative. In other words, O2 is going to be more electron negative. Thus, it is quite likely that at this time ($t\sim 38$), the electronic structure due to tautomerization has changed by passing through an avoided crossing. (Since we traced the dynamics at the Hartree–Fock level, we could not explicitly detect the avoided crossing.) In this way,

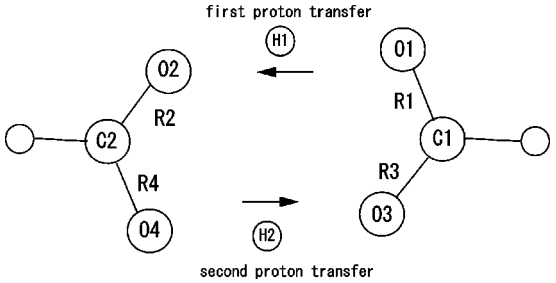

FIG. 8. Definitions of R1, R2, R3, and R4 for the first- and second proton transfers.

C2–O2 turns out to be a single bond and C2–O4 a double bond.

The change of bond nature is also detected in terms of the bond lengths. Figure 9(b) displays the time dependence of the difference R2–R4, where R2 (R4) is R_{C2-O2} (R_{C2-O4}) (see Fig. 8). This figure also indicates that the bond C2–O2 is elongated to be a single bond, whereas C2–O4 is shortened to a double bond at this critical time.

Next, we examine the difference of the electron densities on O3 and O4 sandwiching the second proton in terms of the statistical data. Figure 10(b) exhibits the frequency histogram of $E_{O3}-E_{O4}$ on the occasion of second proton transfer ($\xi_2=0.5$), along with similar data, panel (a), which is $E_{O2}-E_{O1}$ for the first proton transfer ($\xi_1=0.5$). Panel (b) clearly shows that the electron distribution at O3 (proton acceptor) is higher than that of O4 (donor) for the second proton and thereby attracts more strongly. As for the first proton transfer, the gradient of the electric field appears in the other way around. The panel (a) indicates that the electron density on O1 (donor) is higher than that on O2 (acceptor). Thus, the first proton must move against the electric field with the help of concentration of its kinetic energy to the reaction coordinate, as stated in Sec. V A.

D. Donating- and accepting modes of O–C–O skeletons

An application of the RRK (Rice–Ramsperger–Kassel) theory[21] to the present system based on the full statistical assumption has predicted a much longer induction time ($\approx 10^{-7}$ s) for the first proton transfer than the results from actual simulation ($\approx 10^{-14}$ s). The system is hence not fully ergodic. It turns out numerically that only 3 to 4 out of 24 degrees of freedom can be regarded as effectively statistical modes. Unfortunately we cannot currently identify those modes, but they must be related to the motion of protons and antisymmetric stretching of O–C–O bonds.

To investigate the effects of skeleton motion on the DPT process, we examine four different C–O distances, R1, R2, R3, and R4 as defined in Fig. 8. Let us see the geometrical change on the occasion of the first proton transfer, $\xi_1=0.5$. Figures 11(a), 11(b), and 11(c) show the relative length of C–O bonds in terms of the differences (a) R2–R1, (b) R2–R4, and (c) R1–R3. As far as the stable structure is concerned, R2–R1$=-0.1$, R2–R4$=-0.1$, and R1–R3$=0.1$ as shown in Fig. 1. The histograms in Fig. 11 therefore imply that the geometry of the skeletons at the time of the first proton transfer is not much different from the original stable structure. In other words, the first proton is pushed to the other side without large deformation of the skeleton O–C–O bonds.

The geometrical situation on the occasion of the second proton transfer is quite different from the first one, as seen in Fig. 12. It simply claims that at $\xi_2=0.5$ we have R3>R4, R3>R1, and R2>R4. At this moment, the double bond of

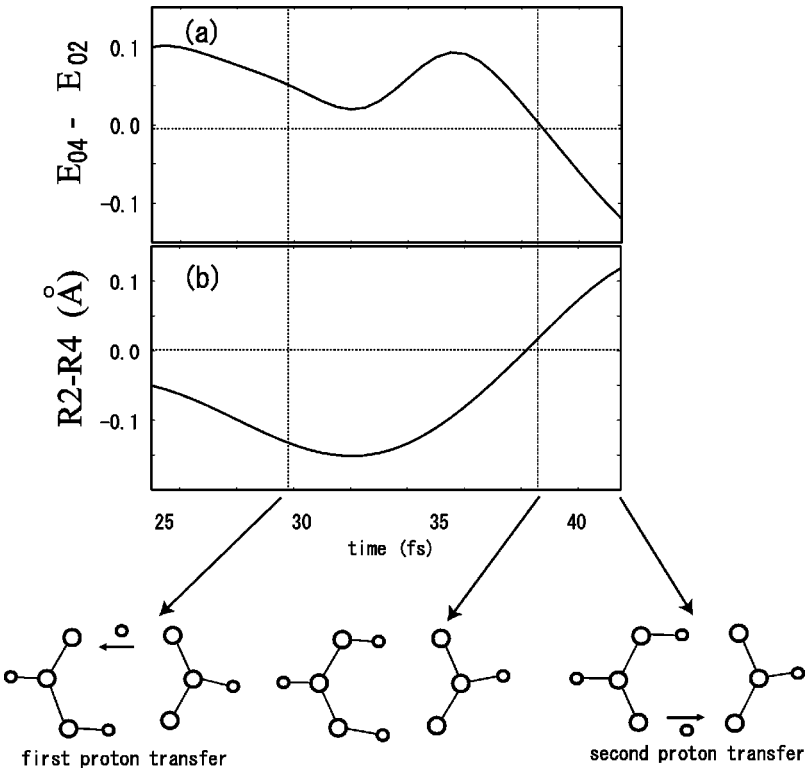

FIG. 9. Difference of the electron densities on the oxygen atoms O4 and O2 in panel (a), and difference of the bond lengths R2–R4 in (b).

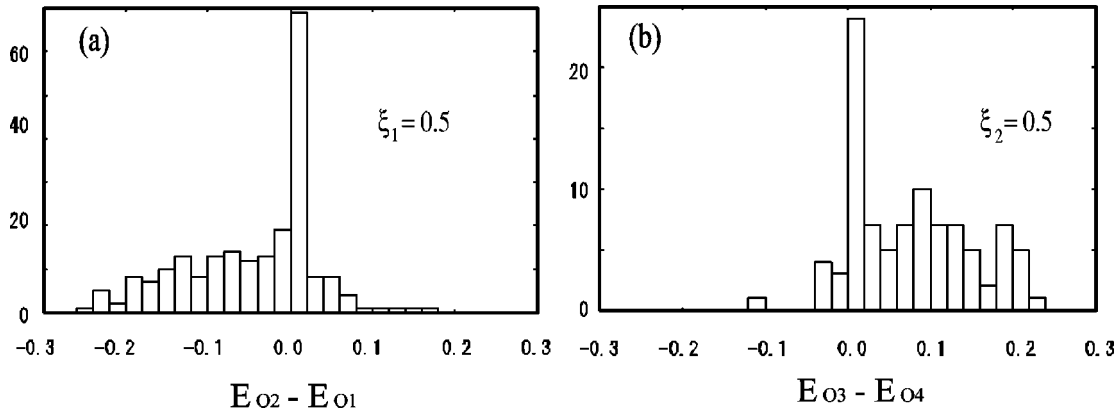

FIG. 10. Frequency histogram of (a) $E_{O2}-E_{O1}$ for the first proton transfer ($\xi_1=0.5$) and (b) $E_{O3}-E_{O4}$ on the occasion of the second proton transfer ($\xi_2=0.5$).

C1–O3, corresponding to R3, has been changed to a single bond to accept the proton, while C2–O4, corresponding to R4, becomes shorter to be a double bond. For these geometrical changes to occur in a synchronous manner, the antisymmetric stretching motions of O2–C2–O4 and O1–C1–O3 seem to be vital. The former deserves to be called a donating mode, and the latter an accepting mode.

If a synchronous configuration of the donating- and accepting modes were not actually realized after the first proton transfer, practically the second proton transfer would not follow. As an example, see Fig. 13, in which R2–R4 is plotted for a case where only a single-proton transfer occurs and this proton eventually returns to the original position. R2 remains shorter than R4 for the single-proton transfer case, while R2 becomes longer than R4 in the case where the double-proton transfer actually takes place.

VI. CONCLUDING REMARKS

We have investigated a full-dimensional *ab initio* dynamics to investigate the mechanism of double-proton transfer in FAD, which serves as one of the simplest models of MPT systems. It turns out that the dynamics and mechanism of double- (or more) proton transfer should not be described in terms of the information of a potential surface alone. For instance, a reaction path based on the optimized energetics favors the simultaneous (synchronous) proton transfers. On the other hand, the sudden approximation suggests a successive mechanism with a high potential barrier. The reality is not as simple as these predictions make it seem.

By studying full-dimensional dynamics, we found that the DPT in FAD does not occur in a concerted manner and is actually associated with a time lag as long as about 8 fs. This value of the average time lag is equivalent to about one-

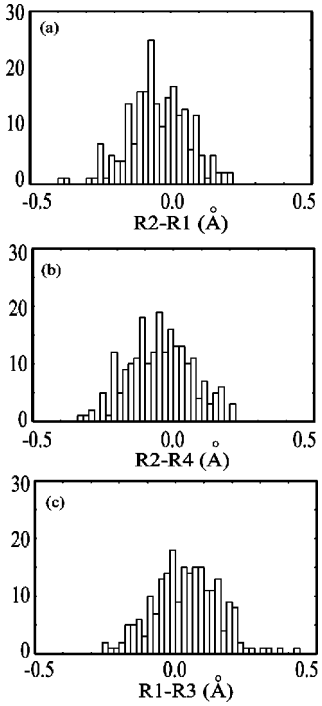

FIG. 11. Balance of the C–O bond lengths at the first proton transfer ($\xi_1=0.5$). (a) R2–R1; (b) R2–R4; and (c) R1–R3.

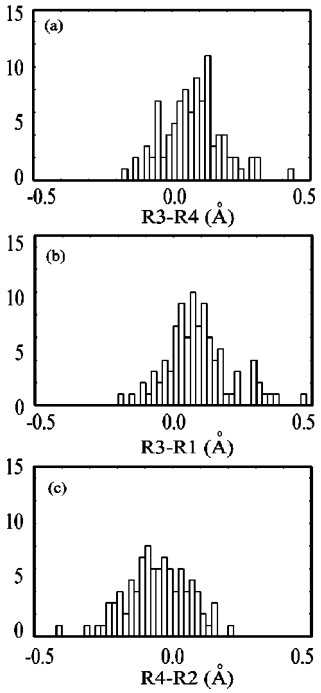

FIG. 12. Balance of the C–O bond lengths at the second proton transfer ($\xi_2=0.5$). (a) R3–R4; (b) R3–R1; and (c) R4–R2.

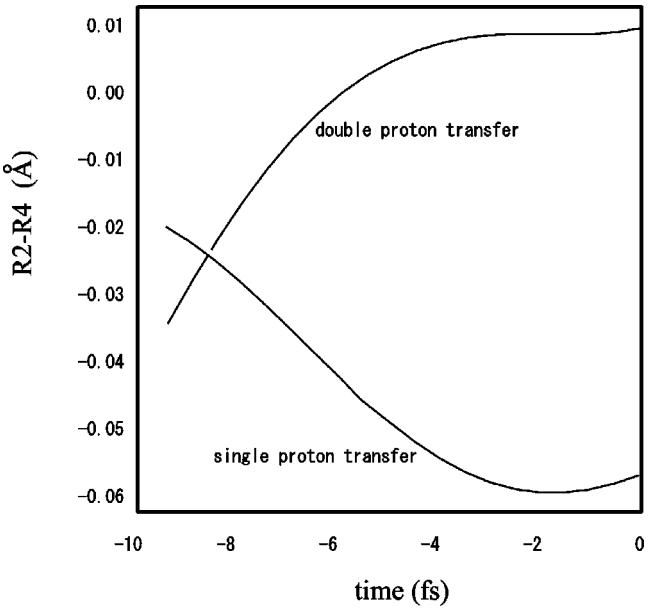

FIG. 13. Differences of CO bond lengths, R2–R4, along paths for single-proton transfer only and double-proton transfer.

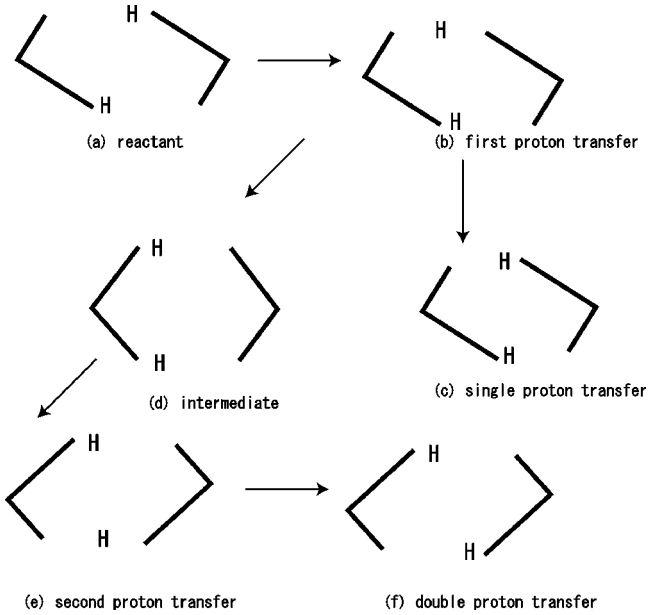

FIG. 14. Schematic picture for the reaction mechanism in FAD.

quarter of the period of C–O vibrational motion. Besides, a clear difference in the mechanism of the first- and second-proton transfers has been identified. We summarize it showing a schematic picture in Fig. 14.

(1) The first proton can undergo a transfer to the other side only when its kinetic energy is directed along the reaction coordinate [Fig. 14(b)]. This motion is thermal and needs a certain activation energy. The reaction rate of the first proton transfer can thus be enhanced by injecting an energy, and this is really the case.
(2) In order for the second proton to make a transfer, geometrical deformation of the O–C–O skeletons is necessary. The length of the C–O bond of the donor side becomes shorter and simultaneously that of the acceptor side turns out to be longer [Fig. 14(e)], which thereby induces a change of the electronic structure (tautomerization), switching the position of the double bond of C═O. It takes on average about 8 fs for this geometrical change to take place, since the period of the C–O bond is about 31 fs. Thus, 8 fs constitutes the time lag between the first- and second-proton transfer. If, on the other hand, the appropriate deformation does not follow the first proton transfer, the second one does not accomplish transfer.
(3) Due to switching of the electronic state induced by the geometrical change of the skeletons, the oxygen of the accepting side of the second proton appears to be more electron rich than the donor oxygen. Thus, the rearrangement of the electronic field pulls the proton in a rather static manner. Since the period of the C–O bonds is not sensitive to the energy change of our focus of interest, the speed of the second proton transfer is not expected to be promoted by increasing the energy, which actually has been confirmed.

An experimental determination of the successive mechanism of the double-proton transfer would still be very difficult, since the time lag (about 8 fs) predicted is too short even for well-advanced experimental techniques to date. However, the essential virtue of the present study is that the difference in the reaction mechanisms of the first- and the second proton transfers has been clarified. This may bring about some qualitative consequences in understanding the dynamics of double-proton transfer. For instance, a solvent effect can have a large difference on the first- and second-proton transfers. The first one will be treated in the theoretical scheme of a rate theory taking account of a heat bath, while the second transfer will be affected by an electronic field modified with the presence of solvent molecules. Also, the effects of quantum tunneling and isotope substitution of one of the protons will reflect the difference of the mechanism.

In this DPT system, quantum-mechanical tunneling is vital. We have already developed a multidimensional semiclassical tunneling theory for large systems,[22] and its application to FAD will be reported elsewhere.[23]

ACKNOWLEDGMENT

This work has been supported in part by a Grant-in-Aid from the Ministry of Education, Science, and Culture of Japan.

[1] *Proton Transfer in Hydrogen-bonded Systems*, edited by T. Bountis (Plenum, New York 1992).
[2] H. H. Limbach and J. Manz, Ber. Bunsenges. Phys. Chem. **102**, 289 (1998).
[3] J. Bertran, A. Oliva, L. Rodrigues-Sabtiago, and M. Sodupe, J. Am. Chem. Soc. **120**, 8159 (1998).
[4] V. A. Benderskii, V. I. Goldanskii, and D. E. Makarov, Phys. Rep. **233**, 195 (1993).
[5] V. A. Benderskii, V. D. E. Makarov, and C. A. Wight, Adv. Chem. Phys. **88**, 1 (1994).
[6] K. Fuke, H. Yoshiuchi, and K. Kaya, J. Phys. Chem. **88**, 5840 (1984); K. Fuke and K. Kaya, *ibid*. **93**, 614 (1989).

[7] M. Chachisvilis, T. Fiebig, A. Douhal, and A. H. Zewail, J. Phys. Chem. A **102**, 669 (1998).
[8] T. Fiebig, M. Chachisvilis, M. Manger, A. H. Zewail, A. Douhal, I. Garcia-Ochoa, and A. de La Hoz Ayuso, J. Phys. Chem. **103**, 7419 (1999).
[9] S. Takeuchi and T. Tahara, Chem. Phys. Lett. **228**, 1 (1998); J. Phys. Chem. **102**, 7740 (1998).
[10] V. Guallar, V. S. Batista, and W. H. Miller, J. Chem. Phys. **110**, 9922 (1999).
[11] S. Hayashi, J. Umemori, S. Kato, and K. Morokuma, J. Phys. Chem. **88**, 1330 (1984).
[12] Y. T. Chang, Y. Yamaguchi, W. H. Miller, and H. F. Schaefer, III, J. Am. Chem. Soc. **109**, 7245 (1987).
[13] N. Shida, P. F. Barbara, and J. Almlöf, J. Chem. Phys. **94**, 3633 (1991).
[14] Y. Kim, J. Am. Chem. Soc. **118**, 1522 (1996).
[15] J-H. Lim, E. K. Lee, and Y. Kim, J. Phys. Chem. A **101**, 2233 (1997).
[16] T. Loerting and K. R. Liedl, J. Am. Chem. Soc. **120**, 12595 (1998).
[17] S. Miura, M. E. Tuckerman, and M. L. Klein, J. Chem. Phys. **109**, 5290 (1998).
[18] P. Jaque and A. Toro-Labbe, J. Phys. Chem. A **104**, 995 (2000).
[19] J. Kohanoff, S. Koval, D. A. Estrin, D. Laria, and Y. Abashkin, J. Chem. Phys. **112**, 9498 (2000).
[20] H. Ushiyama, Y. Arasaki, and K. Takatsuka (to be published).
[21] J. I. Steinfeld, J. S. Francisco, and W. L. Hase, *Chemical Kinetics and Dynamics* (Prentice-Hall, Englewood Cliffs, NJ, 1989).
[22] K. Takatsuka and H. Ushiyama, Phys. Rev. A **51**, 4353 (1995); H. Ushiyama and K. Takatsuka, J. Chem. Phys. **106**, 7023 (1997); **109**, 9664 (1998); K. Takatsuka, H. Ushiyama, and A. Inoue-Ushiyama, Phys. Rep. **322**, 347 (1999).
[23] H. Ushiyama and K. Takatsuka (unpublished).